Characterization of heavily Cu-doped $La_2CuO_{4+\delta}$ by transmission electron microscopy and electron energy loss spectroscopy

Min Gao and L.-M. Peng
Beijing Laboratory of Electron Microscopy, Institute of Physics and Center for Condensed Matter Physics, Chinese Academy of Sciences, 100080 Beijing, People's Republic of China

X. L. Dong, B. R. Zhao, G. D. Liu, and Z. X. Zhao
National Laboratory for Superconductivity, Institute of Physics and Center for Condensed Matter Physics, Chinese Academy of Sciences, 100080 Beijing, People's Republic of China

(Received 31 January 2000; revised manuscript received 20 April 2000)

The techniques of transmission electron microscopy and electron energy loss spectroscopy (EELS) have been used for characterizing heavily Cu-doped polycrystalline $La_2CuO_{4.003}$ (LCO) samples. Semiquantitative and spatially resolved EELS analysis reveals that Cu may be doped into LCO lattice and that Cu doping introduces effectively holes into the sample. At room temperature, the LCO grains were found to phase separate into hole-poor and hole-rich grains, and in hole-rich grains holes were found to have a strong tendency to concentrate and form one-dimensional static ordering with planar domain wall promoted by high-energy electron beam. Two kinds of modulation vectors have been found, they are $1/4\mathbf{b}^* \pm 1/3\mathbf{c}^*$ (with a wavelength $\sim$18.9 Å) and $1/6\mathbf{a}^* \pm 1/3\mathbf{b}^* \pm 1/2\mathbf{c}^*$ (with a wavelength $\sim$12.7 Å). At lower temperatures, sharper and higher-order superlattice reflections were observed, indicating an enhanced charge ordering, and superlattice reflections originating from $1/4\mathbf{b}^* \pm 1/3\mathbf{c}^*$ were found to dominate those originating from $1/6\mathbf{a}^* \pm 1/3\mathbf{b}^* \pm 1/2\mathbf{c}^*$ with a shorter modulation period.

I. INTRODUCTION

Local charge inhomogeneity is an important feature of copper oxide high-T_c superconductors, and this charge inhomogeneity has been regarded by many as a promising clue to understanding high-T_c superconductivity.[1–3] The macroscopic phase separation occurring in $La_2CuO_{4+\delta}$ (LCO), i.e., into oxygen-rich (hole-rich and superconducting) and oxygen-poor (hole-poor and antiferromagnetic) phases at $0.01 < \delta < 0.055$, has been well studied.[4–9] More recently increasing interest has been attracted into the inhomogeneity on a much smaller scale, i.e., the nanometer scale ordering of holes and spins or the stripe phases found in some typical copper oxide superconductors such as $La_{2-x}Sr_xCuO_{4+\delta}$,[10–17] $YBa_2Cu_3O_{7-y}$,[18] $Bi_2Sr_2CaCu_2O_8$,[19] and $La_{2-x}Sr_xNiO_{4+\delta}$,[20–25] the isomorphic system of $La_{2-x}Sr_xCuO_{4+\delta}$. As described by Emery, Kivelson, and Tranquada,[10] a stripe phase is one in which the doped charges are concentrated along spontaneously generated domain walls between antiferromagnetic insulating regions. Physically the stripes are generated as a result of a competition between the clustering tendency of holes and the long-range Coulomb interactions. Many experiments have observed the signature of charge stripes and provided evidences for stripe phases to be closely connected with superconductivity. In general, the stripes of charges and spins are instantaneous and dynamical. It was noted, however, that static stripes are incompatible with the metallic behavior of the cuprates.[12]

Almost all experimental methods which are capable of probing local structural and electronic information have been used for the studies of stripes of charges and spins. These methods include neutron scattering,[10–17,20–25] nuclear magnetic resonance (NMR),[26,27] extended x-ray absorption fine structure (EXAFS),[28–30] x-ray diffraction,[31] angle-resolved photoemission spectroscopy (ARPES),[32] and electron diffraction.[33–35] Among these methods, neutron scattering has been used most successfully for providing evidence for stripes of spins. So far, most neutron-scattering studies, especially those inelastic neutron-scattering studies, have been focusing on the CuO_2 plane, and the observed stripes are regarded as a one-dimensional modulation in a two-dimensional system, i.e., stripes composed of parallel modulating chains on the CuO_2 plane. Although evidences implying correlation along the *c* axis have also been provided by EXAFS measurements,[28–30] this *c*-axis correlation is usually neglected in interpreting experimental results. In this article we will show that the combined techniques of electron diffraction, imaging, and electron energy loss spectroscopy (EELS) in a TEM can be a useful tool for studying charge stripes. High-energy electrons are very sensitive to charge-density modulations and resulting atomic displacement patterns.[36–38] In addition, the high spatial resolution of TEM makes the requirement for the sample quality less strict than that required in neutron diffraction. This is especially important when studying polycrystalline and multiphase samples. Systemic EELS studies by Nücker *et al.* demonstrated that the intensity of a prepeak before the main oxygen *K* absorption edge may be related to the degree of hole doping, and gave a very direct evidence that charge carriers in $La_{2-x}Sr_xCuO_{4+\delta}$ are holes with dominant O $2p$ character.[39] Following their work, the technique of EELS (Ref. 40) has become a widely used tool for the study of local electronic structure of high-T_c superconducting materials[41–46] and other

doped antiferromagnets such as $La_{1-x}Sr_xMnO_3$.[47] In this work, we take advantage of the high spatial resolution of TEM and use the intensity of the hole-related oxygen *K* absorption pre-edge peak as an effective local hole-density detector.[48] The disadvantage of electron diffraction is that it is not sensitive to spin and the technique may therefore not be used for studying the instantaneous stripes of spins. Besides the well-known studies on the charge ordering in $La_{2-x}Sr_xNiO_{4+\delta}$ (Ref. 33) and $La_{1-x}Ca_xMnO_3$,[34,35] some electron-diffraction studies have observed modulation structure in heavily oxygen-doped $La_2CuO_{4+\delta}$ (Refs. 49 and 50) and $La_2NiO_{4+\delta}$.[51–53] Modulations in these materials were attributed to oxygen ordering. It was also pointed out that the original model for the oxygen ordering in $La_2CuO_{4+\delta}$ and $La_2NiO_{4+\delta}$ is not correct.[55,56] A more recent model revealed by neutron diffraction is that the interstitial oxygens order one dimensionally along *c* axis.[56]

We recently observed that phase separation may occur in a Cu-doped $La_2CuO_{4.003}$ sample with nominal ratio [La]:[Cu] = 2:1.06.[57]The interesting point to note is that the excess oxygen value δ in that sample was much less than the low threshold value of 0.01 for phase separation to occur in normal oxygenated $La_2CuO_{4+\delta}$ samples. It was suggested that the excess Cu^{2+} ions (each with a spin of 1/2) substitute the La^{3+} ions (having no spin), the substitution enhancing three-dimensional antiferromagnetic exchange interaction and therefore promoting phase separation via motivating hole segregation. In addition, a modulation structure was observed in this medium Cu-doped sample and this modulation was shown to result from hole ordering.[37] However, very similar modulation has been found in heavily oxygenated $La_2CuO_{4+\delta}$ samples and was attributed to result from the ordering of interstitial oxygen ions.[49,50] In fact, the Cu-doped LCO sample has been studied for more than ten years. Early consensus was that the [La]:[Cu] ratio could not deviate from 2:1 by more than 0.01.[4]

In this paper, we report a detailed TEM and EELS characterization of a heavily Cu-doped $La_2CuO_{4+\delta}$ sample with nominal ratio [La]:[Cu]=2:1.18. A systematic study using XRD and magnetic methods on a series of Cu-doped samples with different [La]/[Cu] ratios revealed that our sample is likely to be a saturated Cu-doped LCO sample.[58] It is the purpose of this paper to examine using TEM based techniques whether the excess Cu atoms have been intercalated into LCO lattice, how the intercalated Cu ions influence the local electronic structure, what is the nature of the modulation we observed, and how holes are distributed in the sample. In this work, normal ([La]:[Cu]=2:1) $La_2CuO_{4+\delta}$ and heavily oxygenated $La_2CuO_{4+\delta}$ samples were also examined and used as references.

II. EXPERIMENT

Polycrystalline $La_2CuO_{4+\delta}$ samples with nominal [La]:[Cu] ratios of 2:1.00 and 2:1.18 were prepared using the conventional solid-state reaction method as described in detail in Ref. 57. The excess oxygen values of these samples δ were determined to be 0.003 by the gas effusion spectra method. The heavily oxygen-rich $La_2CuO_{4.12}$ sample was prepared by the method described by E. Takayama-Muromachi and Narrotsky.[59]

TEM observations were carried out using a field-emission gun (FEG) Philips CM200/FEG (200 keV) and a Philips CM12 (120 keV) transmission electron microscope. EELS experiments were conducted using a Gatan Imaging Filter (GIF) attached to the bottom of the camera chamber of the Philips CM200/FEG electron microscope. The CM12 electron microscope enables a tilt of $\pm 60°$ degree in one direction and $\pm 30°$ in the other vertical direction. A Gatan liquid-nitrogen cooling double-tilt stage (which can vary the temperature between 93 and 373 K) was employed in temperature varying experiments.

III. RESULTS

A. Phase identification and [Cu]/[La]

Based on EELS and selected area electron diffraction (SAED) results, most grains in the polycrystalline Cu-doped samples were determined to be $La_2CuO_{4+\delta}$ (orthorhombic), and minority grains were identified to be monoclinal CuO impurity phase. Based on our TEM observations we estimate that the number of grains with CuO phase was much less than 5% of the total number of grains, and this estimation is consistent with an independent XRD study of the same samples.[58] The two phases may be distinguished readily from their distinct SAED patterns and EELS spectra. Figure 1(a) shows a bright field image of a polycrystalline Cu-doped sample. Among the many grains, a CuO grain was identified and marked in the figure. Corresponding EELS spectra from the LCO and CuO grains are shown in Fig. 1(b). In these spectra O-*K*, La-$M_{4,5}$, and Cu-$L_{2,3}$ edges are clearly visible. The spectrum showing La-$M_{4,5}$ ''white line'' was obtained from LCO grains which distinguishes remarkably from that from CuO grains. In addition, O-*K* edge of LCO only has one main peak, while that of CuO has split peaks [Fig. 2(a)].

Since CuO and LCO phases co-exist in the same TEM sample, we may use CuO (which is well studied) as our reference to measure the absolute value of the LCO O-*K* and Cu-$L_{2,3}$ edges with high accuracy. The CompuStage of our Philips CM200/FEG was utilized to move fast and reliably from one phase to the other. Possible errors in EELS peak positions are estimated to be less than 0.2 eV, and are resulted mainly from two sources (i) energy drift ($<$0.1 eV) during acquiring spectra and (ii) finite dispersion ($\sim$0.1 eV). Figures 2(a) and (b) show the O-*K* and Cu-$L_{2,3}$ absorption edges of CuO and LCO in the Cu-doped sample. No distinct difference was found in the Cu-$L_{2,3}$ edges between spectra obtained from CuO and LCO samples, the edges resulting from the transition from the Cu $2p^{3/2}$ and $2p^{1/2}$ to $3d$ empty states. The Cu-$L_{2,3}$ edges obtained from LCO phase have similar shapes to that from CuO phase, and the same maximum value of L_3 edges at 931.2 eV. The full width at half maximum of the L_3 edge is 1.3 eV for CuO and 1.5 eV for LCO.

An attempt was made to compare the [Cu]/[La] ratios between the normal and Cu-doped LCO samples. In principle, under the nonchanneling and weak diffraction conditions, the integrated counts of the ionization edges of special element should be proportional to its contents, and [Cu]/[La] ratios may be calculated from spectra containing Cu and La ionization edges by following a standard procedure of subtracting background and integrating counts. In our case,

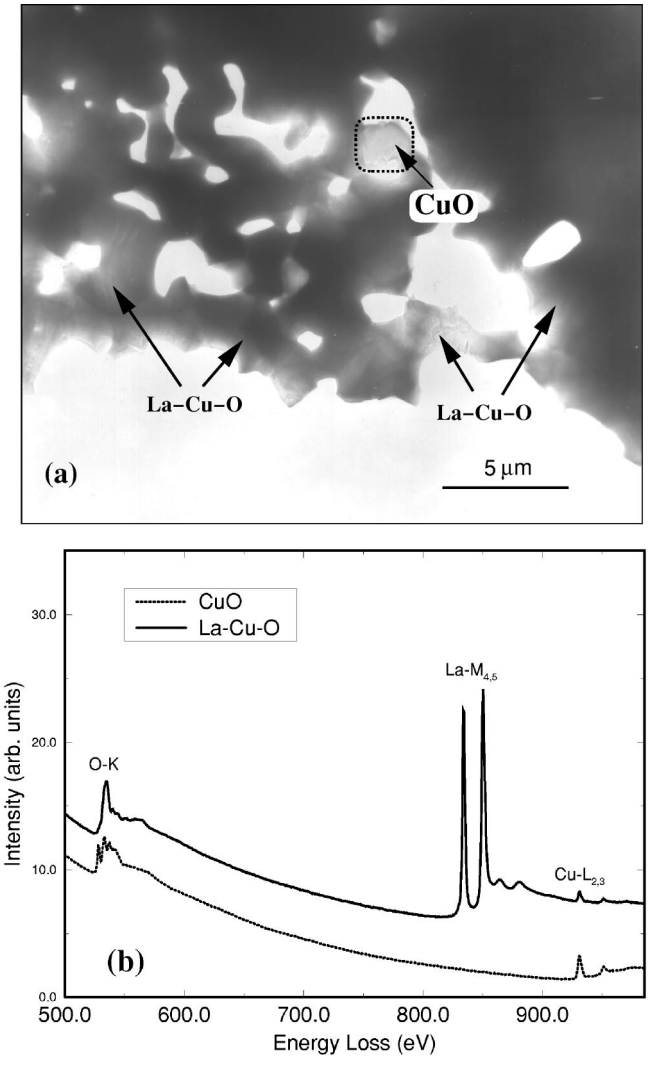

FIG. 1. (a) A bright field image from a heavily Cu-doped $La_2CuO_{4.003}$ sample. A CuO grain is identified. (b) EELS spectra from LCO and CuO phases.

however, the region in between the La-$M_{4,5}$ and Cu-$L_{2,3}$ edges has a badly defined background shape, leading to a considerable error in calculating absolute Cu content. We choose therefore not to determine the absolute La and Cu contents. Instead we aim to compare the [Cu]/[La] ratios of the pure LCO and Cu-doped samples so as to investigate whether additional Cu atoms have been intercalated into the LCO crystal lattice. For this purpose, the ratio between the integrated counts of the Cu-L_3 and La-M_5 peaks was used to represent the [Cu]/[La] ratio. The procedure we used is as follows. First, the La-M_5 edge's background was subtracted by using a standard power-law model.[40] Second, the counts of the La-M_5 and Cu-L_3 peaks were extracted. For the La-M_5 peak, the counts are just the integrated counts over a $\sim$20-eV range centered at the La-M_5 sharp peak. For the Cu-L_3 peak, a simple linear background was assumed near the peak position. The width of integration was chosen to be 9 eV, and the window was centered at the Cu-L_3 peak position. The ratio between the integrated counts of energy windows centered at the Cu-L_3 and La-M_5 peaks is then regarded to represent the [Cu]/[La] ratio. This procedure was applied to spectra obtained from 20 different grains for each

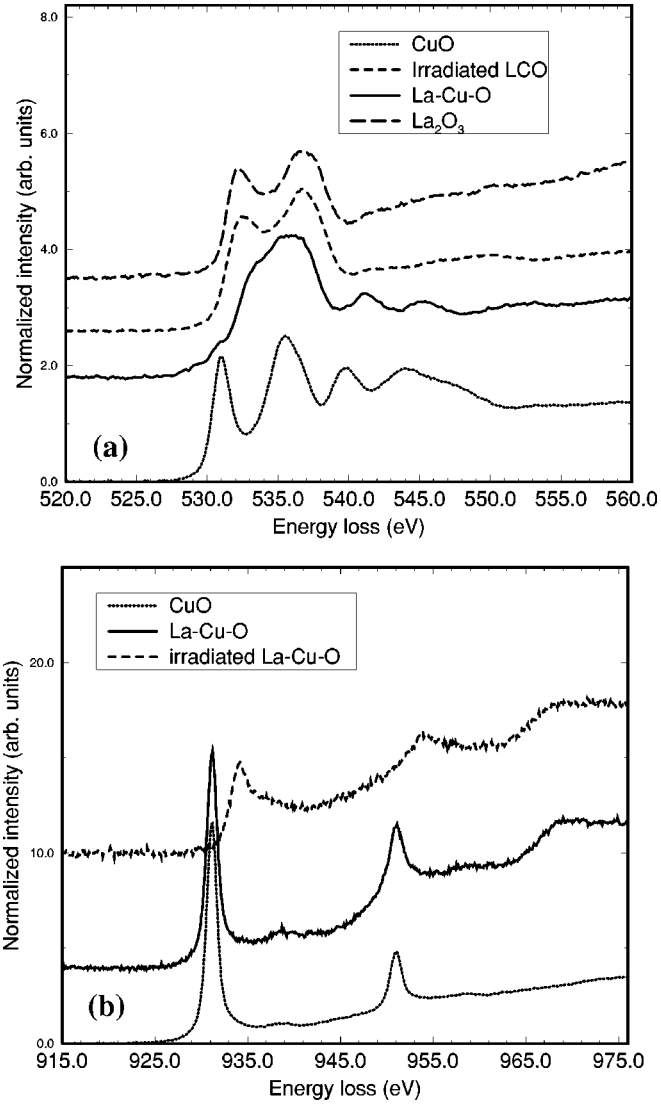

FIG. 2. (a) O-K edges of CuO, LCO, irradiated LCO and polycrystalline La_2O_3. (b) Cu-$L_{2,3}$ edges of CuO, Cu-doped LCO and irradiated LCO.

sample. The average values for normal and Cu-doped samples are, respectively, $0.02\,043 \pm 0.001\,02$ and $0.023\,80 \pm 0.0012$, the error being estimated conservatively to be about 5%. The content of Cu in the Cu-doped sample is therefore estimated to be $16 \pm 8\%$ higher than that in a normal LCO sample. As mentioned earlier that the quantitative procedure we used is not particularly suitable for determining Cu content in the LCO sample. Our results demonstrated, nevertheless, at least qualitatively that additional Cu had been added into the normal LCO lattice. A typical example is shown in Fig. 3, in which two spectra from a normal and a Cu-doped samples are normalized to have the same La-M_5 integrated counts. The magnified Cu-L_3 edges shown as the insert show clearly that the Cu-L_3 edge obtained from the Cu-doped sample is higher than that from the normal LCO sample.

B. Cu-doping effect on O-K absorption edge

For this EELS investigation, each sintered sample was crushed between glass microslides. The resulting powder

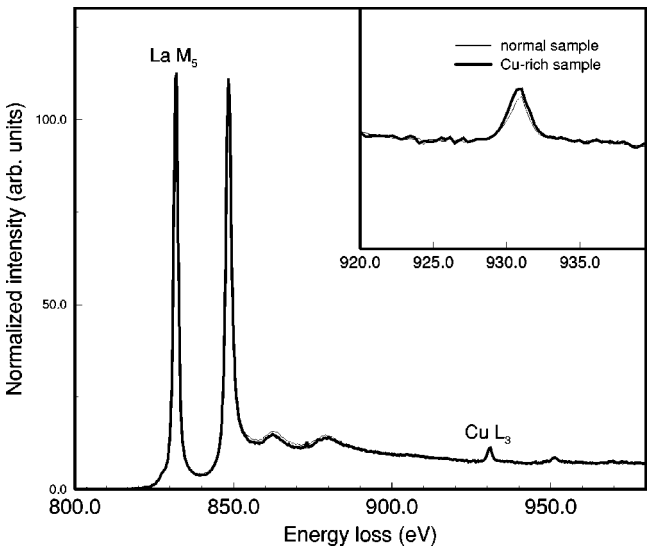

FIG. 3. Typical EELS spectra recorded from Cu-doped LCO and normal LCO samples. The intensities of La-$M_{4,5}$ edges are normalized and the Cu-L_3 edge is magnified.

was spread onto a TEM grid covered with a holy carbon film, and the grid was quickly transferred into the electron microscope. To decrease the effect of electron beam irradiation, the grid was cooled down to ~100 K using liquid-nitrogen cooling stage. Diffraction mode was used and the collection semiangle was set to about 20 mrad. This setup ensured that the dipole law was valid so that for the O-K edge the transition is mainly from $1s$ to $2p$. To minimize dynamical and channeling effects, when recording EELS spectra, LCO grains were so tilted that electrons were incident at the grains along directions which were far from the low-index axes of the grains. The O-K absorption edges of the normal and the Cu-doped samples are shown in Fig. 4. The solid lines are merely guides to the eye. The strong rise of spectral weight above ~531 eV is mainly related to O $2p$ states hybridized with La $5d$ and $4f$ states, i.e., excitations in the LaO layers.[39,42] This main peak seems to be not very different for the two samples. A single pre-edge peak

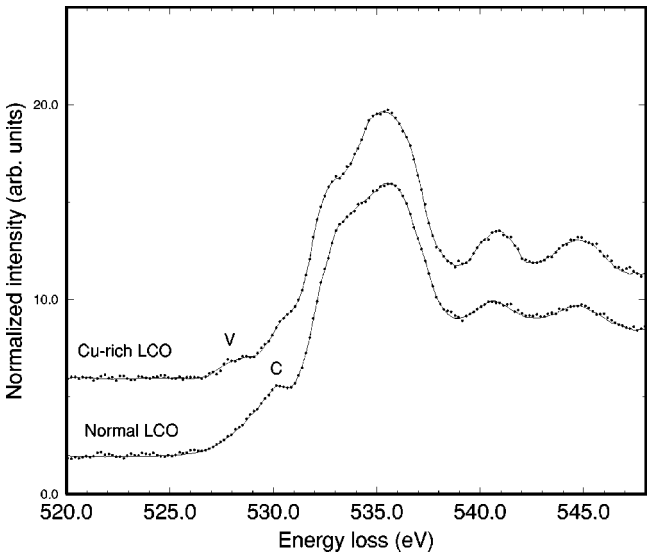

FIG. 4. O-K edges of heavily Cu-doped LCO and normal LCO.

(marked ''C'') with a maximum at ~530.2 eV was observed for the normal sample. Upon doping with Cu, another pre-edge peak ''V'' at ~528.5 eV appeared, and the height of the pre-edge peak C decreased. Similar observations have been reported and the phenomenon has been well studied for $La_{2-x}Sr_xCuO_4$.[39,42] The pre-edge peak ''C'' is attributed to transitions from O $1s$ core state into intrinsic unoccupied O $2p$ states admixed to the conduction band, while the pre-edge peak ''V'' corresponds to the presence of holes at Cu-O plane caused by doping. The spectral weight transfer from the pre-edge peak C to V is characteristic of doped strongly correlated systems.[60] Our results demonstrated that Cu doping introduced holes into the Cu-O layers. The pre-edge peak V of the normal sample is almost invisible in the Cu-doped sample, indicating that the amount of excess O in our sample is very small.

C. Electron irradiation effect on LCO lattice

When illuminated by a 200 keV electron beam with an intensity less than 1×10^{16} nm^{-2}, the Cu-doped LCO sample appeared to be stable. But when the electron-beam intensity was increased to 6×10^{16} nm^{-2}, we found that the LCO grains decomposed quickly under the intense electron irradiation and this phenomenon was best demonstrated from the changes of EELS spectra. Figures 5(a)–(c) show the gradual change of the full spectra including O-K, La-$M_{4,5}$ and Cu-$L_{2,3}$ at low resolution [Fig. 5(a)], O-K edge [Fig. 5(b)], and Cu-$L_{2,3}$ edges [Fig. 5(c)] at higher resolution. From Fig. 5(a) we can calculate the O/La ratios for all spectra. The results are marked in Fig. 5(a). We estimate that the absolute error is about 5% with La_2O_3 as the standard sample, and the relative error should be lower than this value. Figure 5(a) shows that more than 20% O loss had occurred during the electron irradiation process (under constant beam intensity). It was also noted that the La-$M_{4,5}$ edge intensity increased with decreasing O-K edge intensity. Comparing with the first spectrum recorded, the counts of the O-K edge of the last spectrum decreased ~10%, while that of the La-$M_{4,5}$ edge increased ~15%. This situation is similar to what we may expect from a La_2O_3 lattice, in which the atoms per volume of La are about 15.8% higher than that in a La_2CuO_4 lattice, while those of O are about 25.7% lower. Figure 5(b) and 2(a) further show that irradiation caused O-K edge to become a broaden double-peaked structure, and that this edge shape is similar to the O-K edge of a polycrystalline La_2O_3 sample also shown in Fig. 2(a). With increasing irradiation dose, Figs. 5(c) and 2(b) show that both position and shape of Cu-$L_{2,3}$ edge changed. New peaks appeared at about 934 and 954 eV, respectively, and their intensity increased gradually with increasing irradiation dose, while the density of the original Cu-$L_{2,3}$ peak at 931.2 eV faded and disappeared after irradiation. The narrow and sharp $L_{2,3}$ threshold peak of La_2CuO_4 lattice was replaced by a lower and wider peak, which indicated that after electron-beam irradiation the Cu $3d$ band became full. From the position and shape of the Cu-$L_{2,3}$ peaks recorded after irradiation, we conclude that the resulting Cu was in an admixed state of Cu(0) and Cu(I).[61] We propose that the irradiated products are composed of La_2O_3, Cu, and Cu_2O. A possible route leading to these products is that electron-beam irradiation first caused

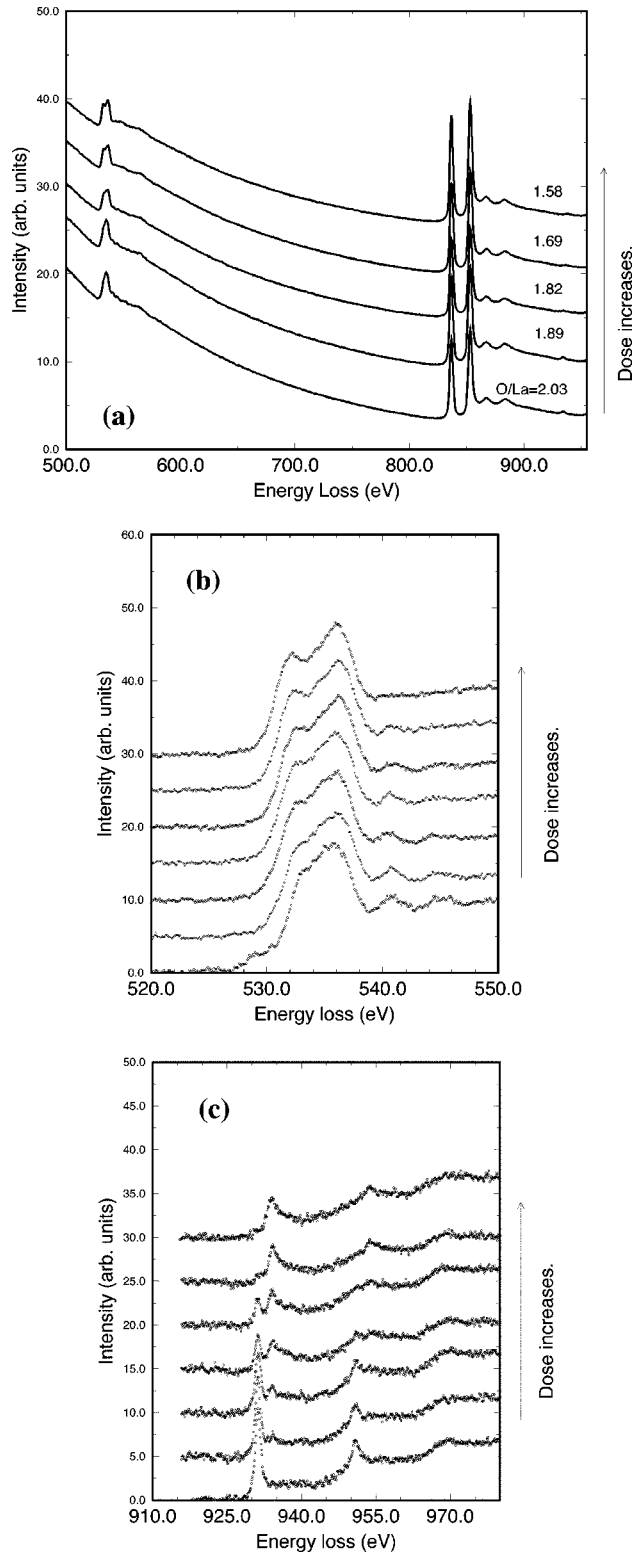

FIG. 5. (a) Irradiation effect on whole spectrum containing O K, La $M_{4,5}$ and Cu $L_{2,3}$. (b) Irradiation effect on O-K edge. (c) Irradiation effect on Cu $L_{2,3}$.

LCO grains to lose oxygen.[45,46] With increasing oxygen losses, the LCO lattice was damaged accompanied by diffusion of Cu atoms to the surface, and LCO crystal transformed to La_2O_3. The final decompositional products may be a layered structure, with the outmost layer being Cu, followed by a Cu_2O layer, and a La_2O_3 layer being in the middle. Under the irradiation of 120-keV electrons, Cu-doped LCO samples appeared to be more stable than under the irradiation of 200-keV electrons.

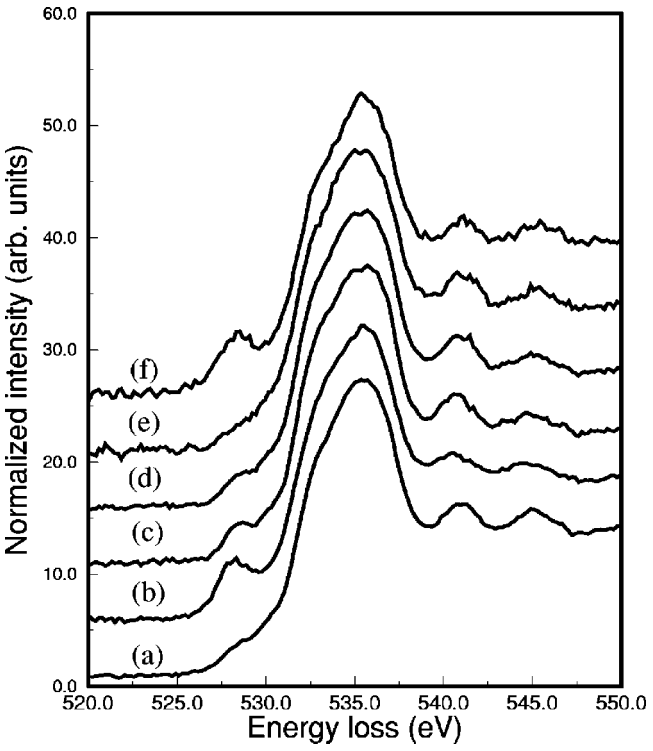

FIG. 6. O-K edges recorded from (a) hole-poor, (b)–(e) hole-rich grains in a Cu-doped polycrystalline LCO sample and (f) from a heavily oxygenated $La_2CuO_{4.12}$.

D. Inhomogeneity of hole distribution at room temperature

We may regard the intensity of the hole-related pre-edge peak ''V'' as a local hole-density detector to measure the hole distribution in the sample. By using an aperture with a size ranging from 200–500 nm to scan on the sample, we are effectively selecting regions contributing to the O-K edges acquired under SAED mode. Local hole densities in different areas were then compared. To avoid the effect of anisotropy on the hole-related pre-edge ''V'' peak intensity, all spectra in Fig. 6 were acquired along [110] axis.

In most LCO grains, the intensities of the pre-edge peak ''V'' were similar to that shown in Fig. 6(a) and this spectrum shows that holes in these grains were resulted mainly from Cu doping. However, in a few grains, much higher pre-edge peak ''V'' were observed, as shown in Figs. 6(b) and (c), suggesting higher local hole densities. Figure 7 shows a TEM image of several LCO grains. Grains 1 and 2 were found to be hole rich, while grains 3 and 4 were found to be hole poor. The orientations of grains 1, 2, and 3 were all near [110], but there existed no definite orientational relationship between them. The thicknesses of grains 1 and 2 were estimated roughly to be in the ranges of 10–100 nm and 100–300 nm, respectively, according to EELS low loss spectra.[40] In the hole-rich grains, most regions had high hole densities as shown in Fig. 6(b). But hole densities in these grains were not uniform, and in some areas, we observed a little lower hole densities as shown in Fig. 6(c). Both Figs. 6(b) and (c) were acquired from grain 1. Figure 6(f) shows

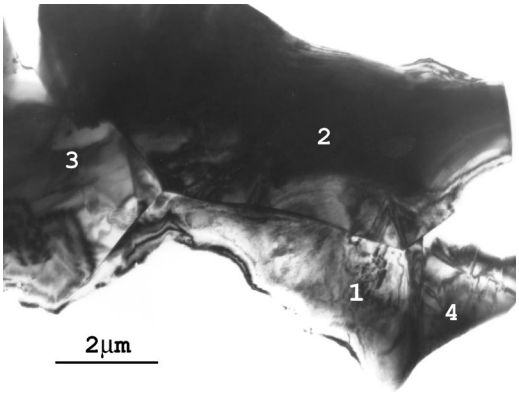

FIG. 7. A bright field image showing a few LCO grains. Grains 1 and 2 shown in the figure are hole rich and grain 3 and 4 are hole poor.

an O-*K* edge acquired from a heavily oxygenated $La_2CuO_{4.12}$ sample at ~100 K. It is seen that the shape of the pre-edge peak ''V'' of Fig. 6(f) is similar to that of Fig. 6(b), both originating from O 2*p* dominated holes on the Cu-O planes. In the heavily oxygenated $La_2CuO_{4.12}$ grains, high density of microstructral defects (especially twins) were found, while hardly any defects were observed in grain 1 and other hole-rich grains in the Cu-doped LCO sample.

Our observations also suggest that the grain boundary seems to act also as boundary for restricting holes in the hole-rich grains. Although we did not find any grain with both hole-rich and hole-poor regions, in the hole-rich grains the hole density was found to be not very homogeneous. We conclude that our Cu-doped $La_2CuO_{4+\delta}$ sample has phase separated into hole-poor and hole-rich grains, and the hole density in the hole-rich grains was not very homogeneous. Our examinations of the polycrystalline sample shows that the number of hole-rich grains is less than about 5% of the total number of grains.

E. Development and characterization of hole modulation structure

In the hole-rich grains and along some special zone axes normal to the *c* axis, such as [100], [110], and [130] zone axes, a modulation structure may sometimes be observed in SAED patterns and an example is shown in Fig. 8(a) which was recorded at RT. In fact, this kind of RT modulation structure was found to develop during our TEM observations, and was not present initially. Figure 9 shows a series

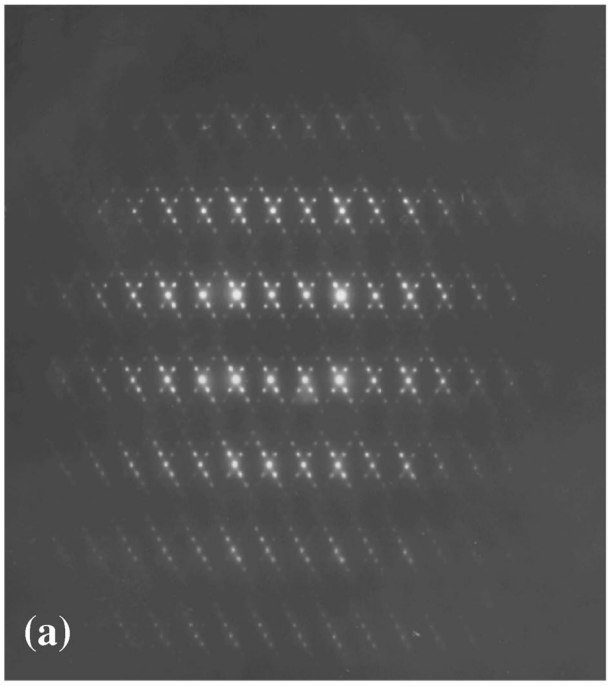

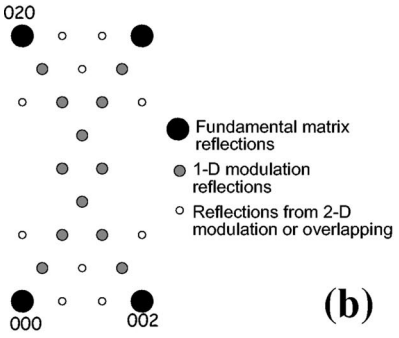

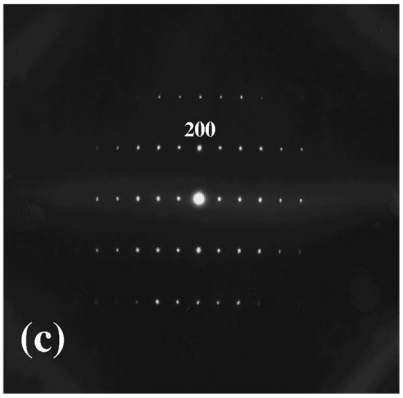

FIG. 8. SAED patterns of (a) [100] and (c) [010] zone axes recorded from a hole-rich grain having modulation structure at RT and (b) a schematic picture of the [100] zone axis diffraction pattern geometry.

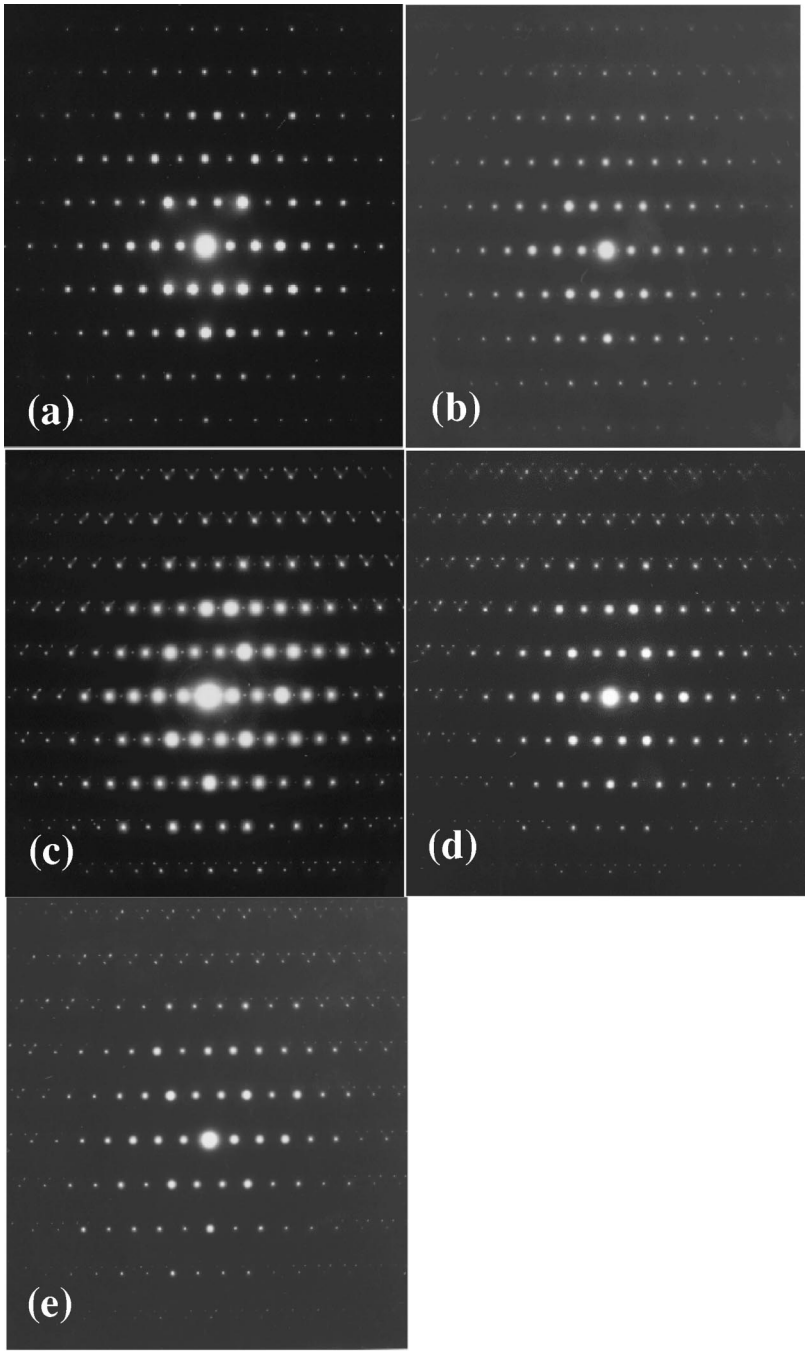

FIG. 9. SAED patterns showing the appearance and development of a static modulation structure: (a) was recorded two minutes after the specimen was exposed to a weak electron beam; (b) was recorded two minutes after (a); (c) was recorded one-half minute after (b); (d) was recorded one half-minute after (c); and (e) was recorded one minute after (d) was recorded.

of *in situ* SAED patterns showing the appearance and development of the modulation structure. It should be noted that the initial [110] SAED pattern [Fig. 9(a)] recorded from a hole-rich grain is the same as that recorded from a hole-poor grain. Only the fundamental Bragg reflections associated with the LCO lattice are present. After exposing the sample to a very weak electron beam for several minutes, superlattice reflections gradually appeared in diffraction patterns recorded from the hole-rich grains, such as Figs. 9(b) and 9(c). Two types of superlattice reflections were found to appear simultaneously. The first type may be written as $(00l)(l=2n+1,n=0,1,2,\ldots)$. It should be noted that these reflections were not expected from both *Bmab* and *Fmmm* space groups so far proposed for the $La_2CuO_{4+\delta}$ lattice. The second type of superlattice reflections may be seen clearly in the outer region of Fig. 9(c) around higher-order matrix reflections. The intensity of $(00l)$ superlattice reflections became very weak [Fig. 9(d)] one minute after it first appeared in Fig. 9(b), and then disappeared completely in Fig. 9(e) which was recorded one minute after Fig. 9(d) was recorded. The other type of superlattice reflections [see Fig. 9(e)] remains strong and stable.

It should be noted that the transition to superstructure was not simultaneous for all hole-rich regions, instead the transition in thick regions (such as in grain 2) was obviously slower than that in thin areas (such as in grain 1). However, even in a thick region, such as in grain 2, the whole transition process finished in less than ten minutes after exposed to the electron beam (which was very weak because the SAED mode was used). In some other hole-rich grains, we observed superlattice reflections directly. This is because by examining one grain we already exposed many other grains near it

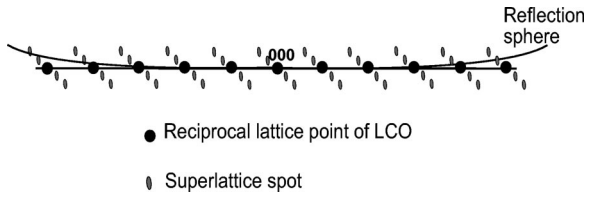

FIG. 10. Schematic diagram showing the generation of superlattice reflections around higher-order main reflections in the outer regions of a [110] SAED pattern.

to electron beam, and in some cases tilting the grains to appropriate zone axis may take more than a few minutes. The reason that we can observe the appearance and development of the superlattice reflections is that it so happened in one of the TEM specimens two hole-rich grains (grain 1 and grain 2 of Fig. 7) were the first and the second grains we observed and they were tilted to [110] axis very quickly.

In general, the superlattice reflections shown in Fig. 9(e) may be written in the form $\mathbf{G}\pm m\mathbf{q}$, and $\mathbf{q}=h\mathbf{a}^*+k\mathbf{b}^*+l\mathbf{c}^*$, where **G** denotes the strong matrix reflections, m is an integer, **q** represents the primary modulation vector, and $\mathbf{a}^*$, $\mathbf{b}^*$, and $\mathbf{c}^*$ are the matrix reciprocal-lattice unit vectors. However, Fig. 9 does not show superlattice reflections of the type $\mathbf{G}-m\mathbf{q}$. Instead superlattice reflections only appear in one side of the main matrix reflections along the direction normal to $\mathbf{c}^*$. This is because the reciprocal plane which contains the modulation vectors is tilted far away from the [110] reciprocal-lattice plane. A schematic diagram is shown in Fig. 10. The main point is that there exists a large angle between the matrix reflections containing reciprocal plane and the line containing the one-dimensional modulation vectors. For the main reflections near (000), the superlattice spots do not intersect with the Ewald sphere. Those around higher-order main reflections may, however, intersect with the Ewald sphere, and this is especially so if the superlattice reflections involve only small angles of scattering and if these reflections are elongated as shown in Fig. 10. For some main reflections **G**, both $\mathbf{G}+\mathbf{q}$ and $\mathbf{G}+\mathbf{2q}$ may be strongly excited. On the other hand, all superlattice reflections of the type $\mathbf{G}-m\mathbf{q}$ lie far outside the Ewald sphere and will not be excited. In all SAED patterns, such as those shown in Figs. 9(b)–(e), superlattice reflections therefore only appear on one side of the main spots. Careful measurements of these superlattice reflections indicate that the modulation first appeared with a $\mathbf{c}^*$ component of $\pm 1/2$ [see Fig. 11(b)]. As the (001) type of reflections faded [Figs. 9(c)–(e)], this component became less than 1/2. This is shown clearer in Figs. 11(a)–(c), which are magnified out regions of Figs. 9(a), (c), and (e).

By systemic tilting experiments the modulation plane was determined to lie in the bc plane. Shown in Figs. 8(a) and (c) are SAED patterns taken along [100] and [010] zone axes and from the hole-rich grain 1. These diffraction patterns shown that both (010)- and (100)-type reflections were absent, indicating that the hole-rich LCO grains with modula-

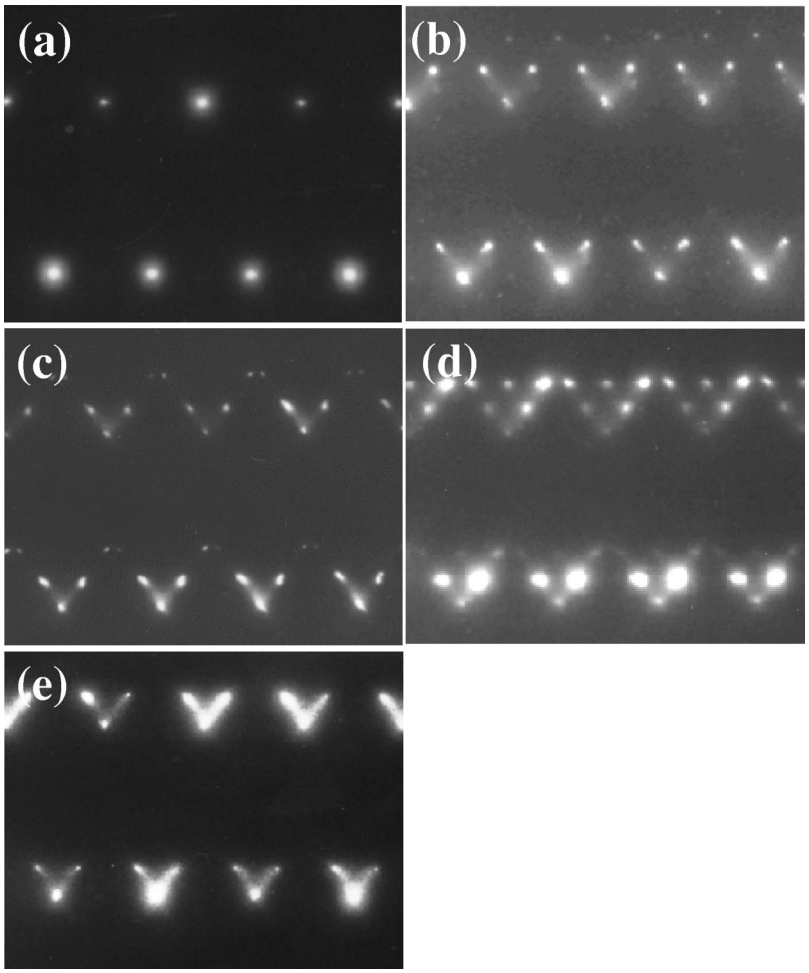

FIG. 11. Magnified partial [110] SAED patterns: (a) part of Fig. 10(a); (b) part of Fig. 10(c); (c) part of Fig. 10(e); (d) part of one at 125 K; (e) part of one after strong irradiation at 200 keV at RT.

tion structure have a space group of *Fmmm*. On the other hand, all hole-poor LCO grains have *Bmab* space group. Figure 8(a) shows two sets of symmetry related modulation superlattice reflections, and Fig. 8(b) shows a schematic picture of this [100] pattern. It should be noted that some features shown schematically in Fig. 8(b) may not be seen easily from Fig. 8(a). Instead they were identified by careful examinations of the negatives of electron diffraction patterns. Figure 8(b) shows graphically that the modulation wave vectors are $\mathbf{q}=1/4\mathbf{b}^*\pm1/3\mathbf{c}^*$ (corresponds to a modulation period $\sim$18.9 Å), i.e., the modulation was commensurate with the LCO lattice.

Figure 8(b) also shows some superlattice reflections (denoted by open circles) which one may expect from a two-dimensional modulation structure or multiple scattering from overlapping domains with different modulation vectors. These reflections, such as $2/3\mathbf{c}^*$ and $1/2\mathbf{b}^*$, may sometimes be observed but are always very weak. This fact suggests that the two sets of equivalent modulation wave vectors came from different domains, and that the modulation in a single domain was a one-dimensional modulation. The existence of these weak superlattice reflections (denoted by open circles) results from multiple scattering of electrons traveling through overlapping domains with different modulation wave vectors. Our result, i.e., reflections denoted by open circles are very weak, suggests that there exists little overlap between domains, which consequently leads to the conclusion that the modulation domain size is typically not much less than the sample thickness. A rough estimation provided earlier about the sample thickness suggests that the domain size is not much smaller than, say, 150 nm.

We have also obtained an independent estimation on the size of the modulation domain as follows. By utilizing the smallest select-area aperture (with a diameter of $\sim$150 nm) to scan over the sample and record SAED patterns from selected regions, we sometimes observed SAED patterns dominated by one set of one-dimensional modulation superlattice reflections. But seldom could we observe only one-directional modulation. This indicated that the size of the domain of one-directional modulation was typically not bigger than the size of the selected area aperture, i.e., 150 nm. Combined with the estimation we obtained earlier, i.e., the domain size cannot be much smaller than 150 nm, because the thicknesses of the grains from which SAED experiments were carried out were not typically not less than 150 nm, we conclude that the modulation domain size is about 150 nm.

F. Electron irradiation effect on the modulation structure and local hole density

Long-time electron irradiation changed local hole density and the modulation structure. We found generally that the lower the electron-beam energy, or the higher the electron-beam intensity, or the larger the sample thickness, the less stable the modulation structure was. Under 200-keV weak electron-beam irradiation, both the modulation structure and hole density in the thin specimen areas remained stable. When the electron-beam flux increased to about 1×10^{16} nm^{-2}, after 10 min irradiation, the modulation became disordered, evidenced in the diffuse intensities in SAED pattern shown in Fig. 11(e). The overall intensity of the modulation superstructure diffraction remained strong, and the corresponding hole density remained high. These results suggest that local hole density was affected less by electron-beam irradiation than the modulation structure, with the former being an integrated quantity while the latter being a spatial distribution of holes. When the beam flux reached 6×10^{16} nm^{-2}, the modulation and the pre-edge peak faded and the LCO lattice was damaged.

Under 120-keV electron-beam irradiation, the modulation structure was much less stable than under 200-keV electrons, and this is true even at very low beam intensity. This damage dependence on the electron-beam energy is opposite to that shown by the LCO lattice, to which damage may be done more easily by higher energy electron beam. At 120-keV, a 10-min irradiation by a strong electron beam may destroy local modulation structure and decrease local hole density substantially. Shown in Fig. 12(a) is a [100] SAED pattern taken from an intensively irradiated region of a hole-rich grain, only very blurred and weak modulation superlattice reflections may still be seen in Fig. 12(a). Figure 12(a) differs from Fig. 8 in that (010) types of reflections now appeared, while these reflections were absent in Fig. 8. The presence of these reflections in Fig. 12(a) indicates that the space group of the corresponding LCO lattice with modulation removed changed into *Bmab*. By long time exposure to weak electron beam, the **c** component of the corresponding modulation wave vector was found to have changed back to 1/2 as shown in Fig. 11(b). An example of so-obtained SAED pattern was shown in Fig. 12(b), together with an enlarged portion shown in Fig. 12(c). Assuming that the two sets of superlattice reflections are symmetry related, the modulation wave vector may then be measured from this pattern to give $\mathbf{q}=1/6\mathbf{a}^*\pm1/3\mathbf{b}^*\pm1/2\mathbf{c}^*$ and a modulation period of $\sim$12.7 Å. Diffraction patterns from [110] zone axis were also obtained, and these pattern are very similar to the one shown in Fig. 9(c).

In order to measure local hole density the sample was quickly transferred from CM12 (in which above-mentioned large tilting experiments were performed) to CM200. The regions showing modulation superlattice reflections were found to have high hole density. Among the two regions showing different modulation wave vectors, the region with a longer period modulation, i.e., a $1/3\mathbf{c}^*$ component, had higher hole density than the one with a shorter modulation period, i.e., a $1/2\mathbf{c}^*$ component. This means that when local hole density decreased, the modulating planes became closer. Figure 6(d) shows a typical O-*K* edge from regions with the $1/2\mathbf{c}^*$ component, and Fig. 6(e) shows the same edge but from a region which was originally hole-rich [see Fig. 11(b)] but became hole poor after exposure to a strong electron beam and showed no modulation superlattice reflections. Comparing with Fig. 5(b), we may conclude that no obvious irradiation damage to the LCO lattice had occurred when recording spectra shown in Figs. 6(d) and (e). Electron-beam irradiation seemed to be able to result in two kinds of domains in one grain: one domain was hole rich, with a space group of *Fmmm* and a modulation structure; the other was hole poor, with a space group of *Bmab* and no modulation structure. The size of these domains was about 100–500 nm. Under the irradiation of both 120- and 200-keV electrons, the modulation structure and local hole density in the thick

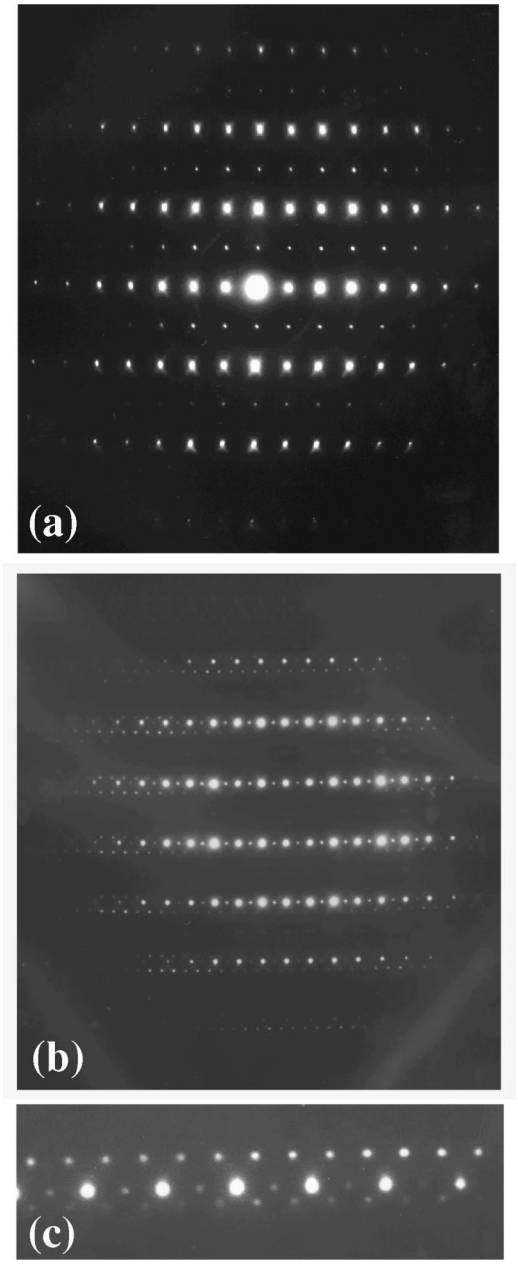

FIG. 12. Irradiation effect on modulation structure. (a) A strong irradiation removed the modulation structure. (b) A weak irradiation changes the modulation vector back to $1/6\mathbf{a}^* \pm 1/3\mathbf{b}^* \pm 1/2\mathbf{c}^*$. (c) Magnified partial pattern of (b).

regions were found to be obviously less stable than that found in thin regions. Long time (hours) exposure to both 120- and 200-keV weak electron-beam irradiation changed the $\mathbf{c}^*$ component of the modulation wave vector from 1/3 to 1/2. The modulation structure then disappeared with decreasing local hole density. When the overall hole density of a hole-rich grain was high, removing the beam from those local regions showing no modulation superlattice reflections or superlattice reflections with a $1/2\mathbf{c}^*$ component for about 30 min, the modulation structure with $1/3\mathbf{c}^*$ component and a space group of *Fmmm* reappeared in the same regions (provided that the nearby region had high density of holes). This indicates that the modulating elements were very mobile. The modulation structure and holes seemed to be mobile only within the grain, and the grain boundary seemed to be a diffuse barrier to holes. A consistent observation is that the originally hole-poor grains 3 and 4 shown in Fig. 8 remained hole poor at all times, and modulation superlattice reflections were never observed from these grains.

G. Effect of temperature on the modulation structure

Low temperature did not cause the modulation wave vector to change noticeably, but it obviously enhanced the modulation. Figure 11(d) shows a portion of a [110] SAED pattern taken from the same area as Fig. 11(c) but at a lower temperature (125 K). The superlattice reflections in general became brighter and sharper, and the SAED pattern contains higher-order superlattice reflections. All these features indicate that the two-dimensional modulation were stronger at lower temperature than at RT. The modulation structure and hole density seemed to be stable at a temperature up to 373 K. We did not observe any visible change at that temperature for 2 h.

H. Summary of experimental results

We now summarize our experimental results presented in the previous subsections. These results are characteristic of the heavily Cu-doped LCO sample and will be referred later in our discussions of these results: (i) There existed a CuO phase in the Cu-doped LCO sample. However, the number of grains with the CuO phase was less than 5% of the total number of grains in the sample. Most of the grains were with the LCO phase. The [Cu]/[La] ratio of the Cu-doped LCO sample was semiquantitatively determined to be higher than that of a normal LCO sample. Cudoping introduced holes into the samples. (ii) Grains in a heavily Cu-doped LCO sample were divided into two groups, i.e., hole-poor and hole-rich grains. Grain boundary seemed to be a barrier for the hole movement. Local hole density in a hole-rich grain was not very homogeneous. (iii) There existed no static observable modulation structure in the hole-rich grains when the sample was first examined. Weak electron beam irradiation caused the formation of static one-dimensional modulation structure at room temperature. In the early stage of the formation of the static modulation structure, the modulation wave vector was found to be $1/6\mathbf{a}^* \pm 1/3\mathbf{b}^* \pm 1/2\mathbf{c}^*$. This modulation wave vector then changed to $q = 1/4\mathbf{b}^* \pm 1/3\mathbf{c}^*$ with a longer period of modulation. The modulation superlattice reflections appeared to be relatively stable under weak electron beam irradiation and at high temperature. The symmetry of grains showing modulation superlattice reflection was *Fmmm*. (iv) The modulation structure and high hole density seemed to be more stable at 200 keV and in thin regions than at 120 keV and in thick areas. High hole density was found to be more stable than the modulation structure. (v) Weak beam irradiation decreased hole density and changed the modulation vector into one with $1/2\mathbf{c}^*$ component. Strong or long-time irradiation removed the modulation and the high hole density and caused a transition of space group of the LCO lattice form *Fmmm* to *Bmab*. (vi) Low temperature enhanced the modulation structure. (vii) Modulating element was found to be mobile. High hole density was always found in areas showing modulation superlattice

reflections. Grain boundaries acted as the barriers to the diffuse of holes and development of modulation structure across grains.

IV. DISCUSSIONS

As discussed above, in a heavily Cu-doped and slightly oxygenated polycrystalline LCO sample, hole-poor and hole-rich grains coexisted at room temperature (RT). This implied that macroscopic phase separation occurred. It was very likely that the hole-rich grains were also oxygen rich. Cu doping generated background holes which were distributed relatively uniform among grains. Additional holes may be introduced by interstitial oxygen ions which may concentrate in a few grains to increase local hole density substantially. Because a large portion of the high-density holes in hole-rich grains was introduced by the excess Cu^{2+} in Cu-doped $La_2CuO_{4+\delta}$ sample, the amount of excess oxygen in a hole-rich grain was then expected to be much less than that expected in the heavily oxygenated $La_2CuO_{4.12}$ sample. This has been demonstrated by the difference in the local defect density found in the two types of samples. Our results indicated that the unit of phase separation in polycrystalline $La_2CuO_{4+\delta}$ was one grain. In addition, local hole density in hole-rich grains was not very homogeneous. The space group of the hole-rich grains showing modulation superlattice reflection was *Fmmm*. With decreasing local hole density and fading of the modulation superlattice reflections, the space group *Fmmm* changed to *Bmab*, the same as that of hole-poor regions.

In hole-rich grains, static modulation structure may be introduced by electron-beam induced effects. In fact, several factors including additional Cu atoms, interstitial O atoms, O vacancies,[62] segregation of additional O atoms into regular shear planes,[63] and holes might contribute to the modulation structure. Noting that this kind of modulation structure cannot be found in hole-poor grains, the possibilities of additional Cu atoms and O vacancies may be excluded. Shear planes may, in principle, produce observable contrasts, but in regions exhibiting modulation superlattice reflections we did not find such contrasts by using both HREM and conventional TEM. On the other hand, the appearance and orientation of both the shear planes shown by Galy[63] and the ordering of oxygen vacancies reported by Tendeloo[62] were different from the modulation found in this study. Furthermore, considering the close relationship between the modulation and local hole density, it can be concluded that the modulation must be hole related. It may result either from the ordering of interstitial oxygen ions or holes or both, while other possibilities can be ruled out. Before Dong *et al.* reported such a modulation in a moderately Cu-doped LCO sample,[57] very similar modulation had been reported to occur in the heavily oxygenated LCO at both 100 K (Ref. 49) and RT.[50] The then-observed modulation structure was attributed to result from the ordering of interstitial oxygen. For a comparison we have also carried out TEM study on a heavily oxygenated $La_2CuO_{4.12}$ sample.[64] According to previous results[49,50,57] and our preliminary results on oxygenated samples,[64] modulation structure found in the oxygenated sample is temperature dependent. At room temperature, the modulation superlattice reflections are very weak, and the modulation wave vector with $1/2\mathbf{c}^*$ component is dominant. At $\sim$100 K, the modulation superlattice reflections become much stronger and the $\mathbf{c}^*$ component of the modulation wave vector becomes smaller, such as 1/3, and corresponding modulation period becomes longer. In the moderately Cu-doped sample the modulation with $1/2\mathbf{c}^*$ component at RT changed to one with a $1/3\mathbf{c}^*$ component at 93 K.[57] In the same reference, it was noted that although the direction of the modulation wave vector changed with varying temperature, the period of modulation remained at approximately 1.9 nm. However, their RT [100] SAED pattern shows that superlattice reflections appear only on one side of the main reflection. According to the analysis given above, this indicated that the modulation wave vector had a component along $\mathbf{a}^*$, which was neglected by Dong *et al.*[57] Considering this $\mathbf{a}^*$ component, the modulation period at 93 K should be longer than that at RT. A general conclusion may therefore be drawn from above discussions that lower temperature enhances the modulation and favors a longer period of modulation. In this study, by using EELS to measure local hole density, we showed that the modulation was also doping dependent. Higher hole density has the same effect on the modulation as lower temperature. These features are contradictory to what one would expect from the model of interstitial oxygen ordering. If the modulation resulted from the ordering of interstitial oxygen ions, local hole density decreases must result from the decreases of density of interstitial oxygen ions, leading to a longer period of modulation. Recent neutron-scattering experiments have revealed the staging behavior of the excess oxygen in $La_2CuO_{4+\delta}$ ($\delta \sim 0.09-0.1$). Excess oxygen atoms tend to form modulation structure along the *c* axis, so the modulation periods is *n* times the spacing between two CuO_2 layers, i.e., half of the *c* axis lattice constant. It was concluded that $n=6$ was at $\delta \sim 0.055$ and $n=4$ is at $\delta \sim 0.11$, and $\delta \propto n^{-1}$ (see Ref. 54). This has also been found to hold for staging in $La_2NiO_{4+\delta}$ by Tranquada *et al.*[56] So we can conclude that the modulation we found in Cu-doped LCO sample is not manifestation of the distortion associated with interstitial oxygen ordering, rather it is the intrinsic response to hole ordering.

This static hole modulation fits the conception of stripe phase described by Emery *et al.* to a certain degree. In the case when $\mathbf{q}=1/4\mathbf{b}^* \pm 1/3\mathbf{c}^*$, high density of holes distributes around the {034} planes with a period which is 12 times the {034} plane spacing. In the planar domain walls, holes seem to distribute uniformly, or three-dimensional modulation structure will form. In addition, the temperature dependence means that the modulation is also controlled by the competition between the clustering tendency of holes and the long-range Coulomb interactions.[10] This static hole ordering is not a confined behavior in CuO_2 layers, but a *c* correlated one-dimensional modulation in a three-dimensional system, i.e., two-dimensional planar domain walls are involved. The period of the modulation increases with increasing hole doping. These features seem to be universal among those static charge ordering observed in doped antiferromagnets.[33,34] In a systematic study on $La_{2-x}Sr_xNiO_{4+\delta}$ (Ref. 33) by electron diffraction, Chen *et al.* reported a charge modulations with similar features. In addition, this static charge ordering in $La_2CuO_{4+\delta}$ can form at RT, which is much higher than that of dynamical stripe phase found by neutron scattering in

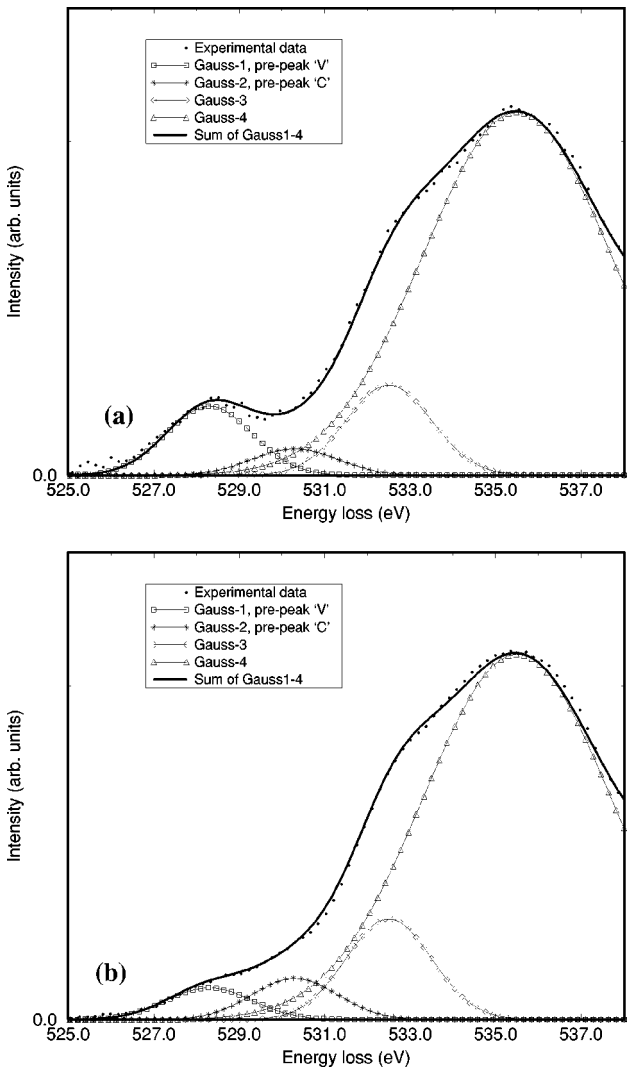

FIG. 13. Fit of the O-*K* edges of hole-poor region of Cu-doped LCO and $La_2CuO_{4.12}$ to obtain the intensities of pre-edge peak V.

other cuprates. EXAFS observed an instantaneous modulation with a modulation wave vector of $0.21\mathbf{b}^* + 1/3\mathbf{c}^*$ in $La_2CuO_{4+\delta}$,[30] which is very similar to what we observed and agrees also with other TEM studies. But this charge ordering could only be observed below 150 K. This implies that the high-energy electrons may prompt holes, which may either distribute homogeneously or form instantaneous stripes, to form static charge ordering. In the early stage of the formation of the static hole stripe, the vector of the stripe changes from $1/6\mathbf{a}^* \pm 1/3\mathbf{b}^* \pm 1/2\mathbf{c}^*$ (corresponding to a modulation period ~12.7 Å) to $1/4\mathbf{b}^* \pm 1/3\mathbf{c}^*$ (corresponding to a modulation period ~18.9 Å). This represents a transition from homogeneous distributed holes to a fully separated hole stripes with high density of holes around the modulating planes or stripes within CuO_2 layers. The vector $1/6\mathbf{a}^* \pm 1/3\mathbf{b}^* \pm 1/2\mathbf{c}^*$ is an intermediate step, and the antiferromagnetic region becomes larger with increasing hole density around each modulating plane. When the local hole density was decreased by electron-beam irradiation, the modulation wave vector changed back to $1/6\mathbf{a}^* \pm 1/3\mathbf{b}^* \pm 1/2\mathbf{c}^*$. This observation indicates that the static stripes can only remain stable near a few special commensurate vectors in the heavily Cu-doped sample. In addition, though the size of the hole-rich regions may be several microns, no uniform modulation exists in a hole-rich grain. A typical condition is that a hole-rich grain is divided into many domains with two equivalent but different vectors and the size of each domain is ~150 nm. This indicates that the modulation is a short-range behavior of holes in doped antiferromagnets.

We have shown that static modulation is not an original feature of the hole-rich grains, but the modulation developed during the observation in TEM. It seems, however, that this modulation is an intrinsic reaction of holes in LCO to high-energy electron beam, i.e., the holes doped into the antiferromagnetic Mott insulator have a strong tendency to congregate and the condition in TEM promotes the formation of static modulation structure. The simplest mechanism for the development of the modulation structure is that the static modulation results from the pinning of dynamical fluctuating stripes by the electron-beam induced effects.[38] Our observations of the development of static modulation structure by TEM has not been confirmed yet by other techniques. Recently a kind of subtle irregular network contrast, universally present in certain zone axis HREM images of $YBa_2Cu_3O_{7-\delta}$ ($\delta < 0.1$), was studied by Etheridge[65] and interpreted as arising from a static local perturbation of the charge-density distribution. The intervals of this kind of structural perturbation were 10–20 Å, similar to the modulation periods found in this study. However, a significant difference exists in both their appearance and characteristics between the two types of superstructures. The structural perturbation studied reported in Ref. 65 did not yield well-defined superlattice reflections, but only very weak diffuse scattering. Moreover, this structural perturbation was argued to be inherent to fully oxygenated $YBa_2Cu_3O_{7-\delta}$ and was not induced under the electron beam.

Our results also indicated that the charge modulation was Cu-doping dependent. In the O-doped normal $La_2CuO_{4+\delta}$, only very weak modulation with $1/2\mathbf{c}^*$ component of modulation wave vector can exist stably at RT. In the moderately Cu-doped $La_2CuO_{4+\delta}$ sample with nominal ratio [La]:[Cu]=2:1.06, at RT a stronger modulation with also $1/2\mathbf{c}^*$ component was shown by Dong *et al.*[57] However, in the heavily Cu-doped sample, at RT, very strong modulation with $1/3\mathbf{c}^*$ has been observed. In fact, this is the first time that a pure $1/3\mathbf{c}^*$ stable modulation in $La_2CuO_{4+\delta}$ at RT has been observed. In previous studies, such a modulation vector can only be found at lower temperature. With the increase of Cu content, the modulation and hole aggregation were enhanced considerably. So Cu doping enhanced the clustering tendency of the holes. This is consistent with the idea that the excess Cu^{2+} ions replace La^{3+} ions.[57] Moreover, because the excess Cu introduced holes, the possibility of interstitial Cu^{2+} can be ruled out. The interstitial Cu can only introduce electrons, not holes. So far, no Cu-doped LCO single crystal has been grown, so it is difficult to directly determine the occupation of the excess Cu. But from above analysis, the excess Cu^{2+} probably replaced La^{3+}. Although quantitative evaluation of the occupation sites of the lowest energy for the excess Cu is beyond the scale of this paper, we may provide a qualitative argument to support our model in which Cu ions replace La ions. In this family of compounds, La vacancies exist. Up to 8% La vacancies have been reported in the related Co-containing compound.[66] If an

excess Cu^{2+} is intercalated into a La vacancy, the strain energy and the electrostatic energy would be reduced, in favor of the model in which Cu ions replace La ions. The excess Cu has been shown to affect the electronic structure and the modulation structure considerably. So it is concluded that the excess Cu value is not very small. Our EELS result showed that the [Cu]/[La] ratio of the heavily Cu-doped sample was $16\% \pm 8\%$ higher than that of the normal sample. By using the ion replacement model (excess Cu^{2+} ions replace La^{3+} ions) and a notation $La_{2-x}Cu_{1+x}O_{4+\delta}$, x value may be calculated to be 0.10 ± 0.05. In addition, x can also be estimated from the intensity of the pre-edge peak ''V.'' Romberg *et al.* have demonstrated that the intensity of the pre-edge peak ''V'' has an approximately linear relationship with the dopant concentration in $La_{2-x}Sr_xCuO_{4+\delta}$.[42] In Fig. 13, the O-*K* edges recorded from hole-poor regions in the Cu-doped sample and that in a heavily oxygenated $La_2CuO_{4.12}$ samples were fitted using several Gauss functions, and the intensities of peak V are extracted. The intensity for the Cu-doped sample is about 6/13 of that of the $La_2CuO_{4.12}$ sample. The hole density of $La_2CuO_{4.12}$ p can be calculated to be 0.175 ± 0.04 according to the relationship $p = 1.3\delta + 0.019$.[67] So the excess Cu can be estimated to be 0.08 ± 0.02 by using the model that one excess Cu ion introduces one hole, in agreement with our estimation based on the [La]/[Cu] ratio method. One remaining question is what causes the modulation superlattice reflected beam intensities. It has been shown that modulated distribution of ions, such as Cu^{+} and O^{-}, can produce enough scattering power at small scattering angles[36,38] so that modulation structure with long periodicity ($\sim$10–20 Å) may be observed.

V. CONCLUSIONS

The heavily Cu-doped and slightly oxygenated polycrystalline $La_2CuO_{4.003}$ sample was found to phase separate into hole-poor and hole-rich grains at RT. Static modulation superstructure was observed to form and develop in hole-rich grains under weak electron-beam irradiation at room temperature. Similar modulation has also been observed in heavily oxygenated and moderately Cu-doped LCO samples. Analyzing synthetically the results of the present study and previous reports on a similar type of modulation, its temperature dependence, hole-density dependence, and Cu-doping dependence were shown. In general, low temperature, high hole density, and high Cu content enhance the modulation and favor a longer period than otherwise. The modulation was concluded to result from charge ordering, and our results agree with the general concept of the stripe phase. The observed evolution of the modulation structure reflects a transition from relatively homogeneously static hole distribution to a fully concentrated hole distribution around a set of modulating planes. The high-density holes have a strong tendency to congregate. The excess Cu^{2+} ions were demonstrated to have been partially intercalated into LCO lattice and probably replaced La^{3+}. These conclusions were derived based on the facts that (i) the [Cu]/[La] ratio of the Cu-doped sample was determined to be higher than that of a normal LCO sample. (ii) The excess holes were shown to have been introduced into CuO_2 planes. (iii) Phase separation and hole ordering occurring in a LCO sample at RT were considerably enhanced by Cu doping.

ACKNOWLEDGMENTS

This work was supported by the National Natural Science Foundation of China and the Chinese Academy of Sciences. We would like to thank Dr. Z. F. Dong, Professor Renhui Wang, and Dr. J. Yuan for valuable discussions.

[1] B.G. Levi, Phys. Today **51** (6), 19 (1998).
[2] Robert F. Service, Science **283**, 1106 (1999).
[3] T. Noda, H. Eisaki, and S. Uchida, Science **286**, 265 (1995).
[4] J.D. Jorgensen, B. Dabrowski, Shiyou Pei, D.G. Hinks, L. Soderholm, B. Morosin, J.E. Schirber, E.L. Venturini, and D.S. Ginley, Phys. Rev. B **38**, 11 337 (1988).
[5] C.D. Castro and M. Grilli, *International School of Solid State Physics, Proceedings of the 3rd Workshop: Phase Separation in Cuprate Superconductors*, edited by K. A. Müller and G. Benedek (World Scientific, Singapore, 1993), p. 12.
[6] R.K. Kremer, V. Hizhnyakov, E. Sigmund, A. Simon, and K.A. Müller, Z. Phys. B **91**, 169 (1993).
[7] V.J. Emery, S.A. Kivelson, and H.Q. Lin, Phys. Rev. Lett. **64**, 475 (1990).
[8] V.J. Emery and S.A. Kivelson, Physica C **209**, 597 (1993).
[9] O. Zachar, S.A. Kivelson, and V.J. Emery, Phys. Rev. B **57**, 1422 (1998).
[10] V. J. Emery, S. A. Kivelson, and J. M. Tranquada, cond-mat/9907228, Proc. Natl. Acad. Sci. USA (to be published), and references therein.
[11] V.J. Emery and S.A. Kivelson, Physica C **263**, 44 (1996).
[12] J.M. Tranquada, B.J. Sternlieb, J.D. Axe, Y. Nakamura, and S. Uchida, Nature (London) **375**, 561 (1995).
[13] P.G. Radaelli, J.D. Jorgensen, A.J. Schultz, B.A. Hunter, J.L. Wagner, F.C. Chou, and D.C. Johnston, Phys. Rev. B **48**, 499 (1993).
[14] B.O. Wells, Y.S. Lee, M.A. Kastner, R.J. Christianson, R.J. Birgeneau, K. Yamada, Y. Endoh, and G. Shirane, Science **277**, 1067 (1997).
[15] S-W. Cheong, G. Aeppli, T.E. Mason, H. Mook, S.M. Hayden, P.C. Canfield, Z. Fisk, K.N. Clausen, and J.L. Martinez, Phys. Rev. Lett. **67**, 1791 (1991).
[16] Y.S. Lee, R.J. Birgeneau, M.A. Kastner, Y. Endoh, S. Wakimoto, K. Yamada, R.W. Erwin, S.-H. Lee, and G. Shirane, Phys. Rev. B **60**, 3643 (1999).
[17] K. Yamada, C.H. Lee, K. Kurahashi, J. Wada, S. Wakimoto, S. Ueki, H. Kimura, Y. Endoh, S. Hosoya, G. Shirane, B.J. Birgeneau, M. Greven, M.A. Kastner, and Y.J. Kim, Phys. Rev. B **57**, 6165 (1998).
[18] H. A. Mook, Pengcheng Dai, S. M. Hayden, G. Aeppli, T. G. Perring, and F. Dogan, Nature (London) **395**, 580 (1998).
[19] H.A. Mook, F. Dogan, and B.C. Chakoumakos,

cond-mat/9811100 (unpublished).
[20] J.M. Tranquada, D.J. Buttrey, V. Sachan, and J.E. Lorenzo, Phys. Rev. Lett. **73**, 1003 (1994).
[21] J.M. Tranquada, J.E. Lorenzo, D.J. Buttrey, and V. Sachan, Phys. Rev. B **52**, 3581 (1995).
[22] J.M. Tranquada, D.J. Buttrey, and V. Sachan, Phys. Rev. B **54**, 12 318 (1996).
[23] P. Wochner, J.M. Tranquada, D.J. Buttrey, and V. Sachan, Phys. Rev. B **57**, 1066 (1998).
[24] S.M. Hayden, G.H. Lander, J. Zarestky, P.J. Brown, C. Stassis, P. Metcalf, and J.M. Honig, Phys. Rev. Lett. **68**, 1061 (1992).
[25] V. Sachan, D.J. Buttrey, J.M. Tranquada, J.E. Lorenzo, and G. Shirane, Phys. Rev. B **51**, 12 742 (1995).
[26] P.C. Hammel, A.P. Reyes, S-W. Cheong, Z. Fisk, and J.E. Schirber, Phys. Rev. Lett. **71**, 440 (1993).
[27] A.W. Hunt, P.M. Singer, K.R. Thurber, and T. Imai, Phys. Rev. Lett. **82**, 4300 (1999).
[28] A. Bianconi, N.L. Saini, A. Lanzara, M. Missori, T. Rossetti, H. Oyanagi, H. Yamaguchi, O. Oka, and T. Ito, Phys. Rev. Lett. **76**, 3412 (1996).
[29] A. Lanzara, N.L. Saini, A. Bianconi, F.C. Chou, and D.C. Johnston, Physica C **296**, 7 (1998).
[30] A. Lanzara, N.L. Saini, A. Bianconi, J.L. Hazemann, Y. Soldo, F.C. Chou, and D.C. Johnston, Phys. Rev. B **55**, 9120 (1997).
[31] M.V. Zimmermann, A. Vigliante, T. Niemöller, N. Ichikawa, T. Frello, J. Madsen, P. Wochner, S. Uchida, N.H. Andersen, J.M. Tranquanda, D. Gibbs, and R. Schneider, Europhys. Lett. **41**, 629 (1998).
[32] Z.J. Zhou, P. Bogdanov, S.A. Kellar, T. Noda, H. Eisaki, S. Uchida, Z. Hussain, and Z.-X. Shen, Science **286**, 268 (1999).
[33] C.H. Chen, S-W. Cheong, and A.S. Cooper, Phys. Rev. Lett. **71**, 2461 (1993).
[34] C.H. Chen, S-W. Cheong, and H.Y. Hwang, J. Appl. Phys. **81**, 4326 (1997).
[35] S. Mori, C.H. Chen, and S-W. Cheong, Nature (London) **392**, 473 (1998).
[36] L. Wu, Y. Zhu, and J. Tafto, Micron **30**, 357 (1999).
[37] L.-M. Peng, Z.F. Dong, X.L. Dong, B.R. Zhao, X.F. Duan, and Z.X. Zhao, Micron **31**, 551 (2000).
[38] L.-M. Peng, M. Gao, Z. F. Dong, X. L. Dong, B. R. Zhao, and Z. X. Zhao, Phys. Rev. B **62**, 189 (2000).
[39] N. Nücker, J. Fink, J.C. Fuggle, P.J. Durham, and W.M. Temmerman, Phys. Rev. B **37**, 5158 (1988).
[40] R.F. Egerton, *Electron Energy-Loss Spectroscopy in the Electron Microscope*, 2nd ed. (Plenum Press, New York, 1996).
[41] C.P. Poole, H.A. Farach and R.J. Creswick, *Superconductivity* (Academic Press, New York, 1995), p. 522.
[42] H. Romberg, M. Alexander, N. Nücker, P. Adelmann, and J. Fink, Phys. Rev. B **42**, 8768 (1990).
[43] J. Yuan, L.M. Brown, W.Y. Liang, R.S. Liu, and P.P. Edwards, Phys. Rev. B **43**, 8030 (1991).
[44] M. Alexander, H. Romberg, N. Nüker, P. Adelmann, J. Fink, J.T. Markert, M.B. Maple, S. Uchida, H. Takagi, Y. Tokura, A.C.W.P. James, and D.W. Murphy, Phys. Rev. B **43**, 333 (1991).
[45] N.D. Browning, J. Yuan, and L.M. Brown, Inst. Phys. Conf. Ser. **119**, 283 (1991).
[46] N.D. Browning, J. Yuan, and L.M. Brown, Supercond. Sci. Technol. **4**, S346 (1991).
[47] H.L. Ju, H.-C. Sohn, and K.M. Krishnan, Phys. Rev. Lett. **79**, 3230 (1997).
[48] Z.F. Dong, L.-M. Peng, X.F. Duan, X.L. Dong, B.R. Zhao, Z.X. Zhao, J. Yuan, and R.H. Wang, Phys. Rev. B **59**, 3489 (1999).
[49] E. Takayama-Muromachi, T. Sasaki, and Y. Matsui, Physica C **207**, 97 (1993).
[50] N. Lagueyte, F. Weill, A. Wattiaux, and J.C. Grenier, Eur. J. Solid State Inorg. Chem. **30**, 857 (1993).
[51] L.C. Otero-Diaz, A.R. Landa, F. Fernandez, R. Saez-Puche, R. Withers, and B.G. Hyde, J. Solid State Chem. **97**, 443 (1992).
[52] A. Demourgues, F. Weill, J.C. Grenier, A. Wattiaux, and M. Pouchard, Physica C **192**, 425 (1992).
[53] Z. Hiroi, T. Obata, M. Takano, and Y. Bando, Phys. Rev. B **41**, 11 665 (1990).
[54] P. Blakeslee, R.J. Birgeneau, F.C. Chou, R. Christianson, M.A. Kastner, Y.S. Lee, and B.O. Wells, Phys. Rev. B **57**, 13 915 (1998).
[55] X. Xiong, P. Wochner, S.C. Moss, Y. Cao, K. Koga, and M. Fujita, Phys. Rev. Lett. **76**, 2997 (1996).
[56] J.M. Tranquada, Y. Kong, J.E. Lorenzo, D.J. Buttrey, D.E. Rice, and V. Sachan, Phys. Rev. B **50**, 6340 (1994).
[57] X.L. Dong, Z.F. Dong, B.R. Zhao, Z.X. Zhao, X.F. Duan, L.-M. Peng, W.W. Huang, B. Xu, Y.Z. Zhang, S.Q. Guo, L.H. Zhao, and L. Li, Phys. Rev. Lett. **80**, 2701 (1998).
[58] X. L. Dong, P. S. Luo, M. Gao, L.-M. Peng, B. R. Zhao, and Z. X. Zhao (unpublished).
[59] E. Takayama-Muromachi and A. Narrotsky, Physica C **218**, 164 (1993).
[60] H. Eskes, M.B.J. Meinders, and G.A. Sawatzky, Phys. Rev. Lett. **67**, 1035 (1991).
[61] G.A. Botton, C.B. Boothroyd, A.U. Hamid, S.B. Newcomb, and W.M. Stobbs, Inst. Phys. Conf. Ser. **138**, 43 (1993).
[62] G. Van Tendeloo and S. Amelinckx, Physica C **176**, 575 (1991).
[63] J. Galy, Acta Crystallogr., Sect. B: Struct. Sci. **B48**, 777 (1992).
[64] M. Gao, G. D. Liu, L. M. Peng, G. C. Che, and Z. X. Zhao (unpublished).
[65] J. Etheridge, Philos. Mag. A **73**, 643 (1996).
[66] J.T. Lewandowski, R.A. Beyerlein, J.M. Longo, and R.A. McCauley, J. Am. Ceram. Soc. **69**, 699 (1986).
[67] Z.G. Li, H.H. Feng, Z.Y. Yang, A. Hamed, S.T. Ting, P.H. Hor, S. Bhavaraju, J.F. DiCarlo, and A.J. Jacobson, Phys. Rev. Lett. **77**, 5413 (1996).